

# **JGR** Earth Surface

## <del>-</del>

#### RESEARCH ARTICLE

10.1029/2024JF007721

#### **Key Points:**

- Bedrock erosion downstream of glaciers is damped through an increase in sediment cover effect caused by glacier-produced sediment
- Basin-wide sediment flux is similar to unglaciated sediment flux at timescales of >100 ky
- Glacially derived bedload provides a missing link between rapid bedrock erosion rates and steady basin accumulation and weathering rates

#### **Supporting Information:**

Supporting Information may be found in the online version of this article.

#### Correspondence to:

S. A. Schanz, sschanz@coloradocollege.edu

#### Citation:

Schanz, S. A., & Yanites, B. J. (2024). Reconciling rapid glacial erosion and steady basin accumulation rates in the late Cenozoic through the effect of glacial sediment on fluvial erosion. *Journal of Geophysical Research: Earth Surface*, 129, e2024JF007721. https://doi.org/10.1029/2024JF007721

Received 1 MAR 2024 Accepted 12 AUG 2024

#### **Author Contributions:**

Conceptualization: Brian J. Yanites Investigation: Sarah A. Schanz Methodology: Sarah A. Schanz, Brian J. Yanites

**Software:** Sarah A. Schanz, Brian J. Yanites **Visualization:** Sarah A. Schanz

Writing – original draft: Sarah A. Schanz Writing – review & editing: Sarah A. Schanz, Brian J. Yanites

© 2024 The Author(s).

This is an open access article under the terms of the Creative Commons

Attribution-NonCommercial License, which permits use, distribution and reproduction in any medium, provided the original work is properly cited and is not used for commercial purposes.

## Reconciling Rapid Glacial Erosion and Steady Basin Accumulation Rates in the Late Cenozoic Through the Effect of Glacial Sediment on Fluvial Erosion

Sarah A. Schanz<sup>1</sup> and Brian J. Yanites<sup>2</sup>

<sup>1</sup>Geology Department, Colorado College, Colorado Springs, CO, USA, <sup>2</sup>Department of Earth and Atmospheric Sciences, Indiana University, Bloomington, IN, USA

**Abstract** The onset of glaciation in the late Cenozoic caused rapid bedrock erosion above the snowline; however, whether the influx of eroded sediment is recorded in continental weathering and basin accumulation rates is an ongoing debate. We propose that the transport of glacially eroded bedrock through the fluvial system damps the signal of rapid headwater erosion and results in steady basin-integrated sediment flux. Using a numerical model with integrated glacial and fluvial erosion, we find that headwater bedrock erosion rates increase rapidly at the onset of glaciation and continue to fluctuate with climatic oscillation. However, bedrock erosion rates decrease in the downstream fluvial system because larger grain sizes from glaciers result in an increase in sediment cover effect. When erosion and sediment flux rates are averaged, long-term sediment flux is similar to nonglacial flux values, while localized bedrock erosion rates in the glaciated landscape are elevated 2–4 times compared to nonglacial values. Our simulated values are consistent with field measurements of headwater bedrock erosion, and the pattern of sediment flux and fluvial erosion matches paraglacial theory and terrace aggradation records. Thus, we emphasize that the bedload produced from glacial erosion provides a missing link to reconcile late Cenozoic erosion records.

Plain Language Summary Glaciers are effective erosion agents and the start of mountain glaciation is thought to correspond to higher alpine erosion rates. However, at the landscape-scale, there is little to no change in erosion rates across the start of glaciation. In order to connect across these scales, we use a computer model to calculate erosion rates and sediment transfer rates. We find that the increase in sediment size from glaciation will lower erosion rates in rivers. Larger sediment sits on the riverbed and protects the underlying rock from erosion. Despite rapid erosion by glaciers upstream of the river, the slower erosion rates in the river result in a constant rate of sediment transferred out. Therefore, sediment transfer from glacier to river systems is an important process for understanding erosion across landscape scales.

#### 1. Introduction

Our understanding of landscape response to late Cenozoic climate change, namely the onset of alpine glaciation, is confounded by conflicting observations. Point measurements of erosion rates in high elevation and glaciated regions show significant increases in bedrock erosion rates and sediment production (Herman et al., 2013; Shuster et al., 2005), whereas geochemical proxies (Lenard et al., 2020; Willenbring & von Blanckenburg, 2010) show little change in long-term denudation rates. In contrast, accumulation curves in oceanic and sedimentary basins suggest an increase in depositional rates coeval with the onset of glaciation (Hay et al., 1988; Molnar, 2004). While both hypotheses are rooted in empirical observations, these data sets measure different spatial and temporal scales of erosion. As such, these opposing observations have not been reconciled. One potential mechanism to reconcile these hypotheses that has yet to be explored is the downstream impact of glacial sediment on fluvial erosion processes. Specifically, we seek to explore the role of glacially derived sediment in covering bedrock from fluvial incision (Cowie et al., 2008; Sklar & Dietrich, 2001) and lowering landscape erosion rates downstream of glacial activity.

High rates of bedrock erosion due to glaciation creates trimmed topography, termed the 'buzzsaw effect', that is observed globally (Egholm et al., 2009; Pedersen et al., 2010). Regionally, glaciated orogens show a correspondence in high frequency elevations, snowline altitudes, and equilibrium line altitudes (ELAs) in the Himalayas (Brozović et al., 1997), Andes (Montgomery et al., 2001), Sierra Nevada (Brocklehurst & Whipple, 2002), and Cascade Range (Mitchell & Montgomery, 2006). These topographic trends for a glacial buzzsaw

SCHANZ AND YANITES 1 of 16

are supported by numerical models (e.g., Egholm et al., 2009) as well as thermochronometric data from glaciated areas, which tend to show an increase in exhumation rates over the late Cenozoic (Herman et al., 2013). For example, data in the Southern Coast Range of British Columbia revealed a >6-fold increase in erosion rates, coincident with the onset of erosive ice sheets at  $1.8 \pm 0.2$  Ma, that lasts for 0.4 Ma (Shuster et al., 2005), and cooling ages associated with rapid denudation of 4-5 mm/yr are co-located with ELAs in southern Alaska, US (Berger & Spotila, 2008).

The strong correspondence between glacial ELA, exhumation rates, and topography implies that glacial erosion rates are enhanced near the ELA, which in turn is controlled by regional and global climate. This link between erosion and climate has been used to explain late Cenozoic increases in erosion rates and associated downstream basin accumulation (Molnar, 2004). Accumulation rates in the last 5 My for oceanic basins are nearly twice as high as any prior period, even when subduction of older basins is accounted for (Hay et al., 1988; Molnar, 2004). Continental basins and mountains also record increased accumulation rates at this time, suggesting that the cause is not related to eustasy (Herman et al., 2013; Molnar, 2004). There was little to no increase in accumulation rates near the tropics, which combined with a lack of a global increase in tectonic activity (Rowley, 2002; Van Der Meer et al., 2014) led researchers to suggest that increased amplitude and frequency of glaciations led to increased erosion and accumulation (e.g., Pedersen & Egholm, 2013).

However, increased erosion cannot be sustained for long before a new topographic equilibrium is achieved; observations of decoupled erosion rates and tectonics tend to last on the order of  $10^6$  years or less (Koppes & Montgomery, 2009; Whipple, 2009). Willenbring and Jerolmack (2016) suggest that erosion rates have actually been steady for the last 10 My; isotopic signatures of silicate weathering are steady over the last 10 My (Willenbring & von Blanckenburg, 2010), in contrast to inferred 2–4 fold increases in weathering based on accumulation rates (Peizhen et al., 2001). Cosmogenic isotopes in Himalayan sedimentary basins indicate steady erosion rates over the late Miocene to present (Lenard et al., 2020). These recent observations suggest that the previously estimated increases in late Cenozoic accumulation rates are potentially biased by the Sadler effect, in which recent events are over-represented in the sedimentary record due to the unsteady nature of erosion and deposition (Sadler, 1981). An updated estimate of sediment accumulation on continental shelves indicates steady rates over the last tens of millions of years (Sadler & Jerolmack, 2015).

One possible mechanism to reconcile the contradiction of locally increased erosion rates and integrated continental-scale steadiness in accumulation and weathering rates is to consider the longitudinal effects of glacial bedrock erosion. An increase in bedrock erosion and sediment production in the headwaters produces sediment that can cover bedrock and damp erosion rates (Sklar & Dietrich, 2001) downstream of the glacially impacted area, potentially balancing the increase in bedrock erosion upstream.

We propose and test the hypothesis that although glacial erosion is more efficient than fluvial erosion in steep landscapes, the resulting increase in sediment production decreases erosion downstream of the glacial extent, which results in overall less mass transported out of the purely fluvial parts of the landscape. Such a process would dampen and perhaps reverse any upland signal of increased sediment production in depositional basins and possibly skew continental-scale weathering estimates (e.g., Willenbring & Jerolmack, 2016). Glacial erosion, in contrast to fluvial erosion, produces sediment that is commonly coarser and in greater supply (Hallet et al., 1996), which could further exacerbate downstream deposition and aggradation. Cycles of fluvial aggradation and incision caused by glacial cycles are well documented in river terrace records (e.g., Hancock & Anderson, 2002; Pan et al., 2003; Pazzaglia & Brandon, 2001), but the effect on total erosion and sediment flux has not been analyzed. We test our hypothesis using a coupled glacial-fluvial 1-D numerical model to quantify how glacially derived sediment affects topographic development, bedrock erosion rates, and sediment fluxes in mountainous environments.

## 2. Methods

We built a numerical model that integrates one-dimensional (1-D) glacial (MacGregor et al., 2000) and fluvial (Campforts et al., 2020; Shobe et al., 2017; Yanites, 2018) erosion models, with feedbacks in place for sediment and water transfer (Figure 1). Although the model is 1-D, valley width is tracked and sediment is stored across the valley in order to simulate glacial sediment storage. The model is 200 km long with computational nodes every 2 km; this spacing was necessary for sediment transport stability at a timestep of 1 year (Text S4 in Supporting Information S1). The major components of the model are detailed below and include bedrock incision, sediment

SCHANZ AND YANITES 2 of 16

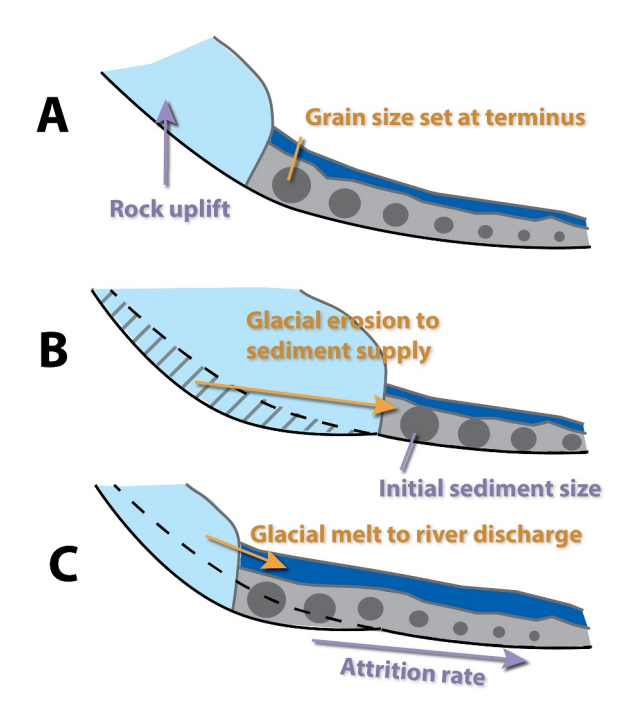


**Figure 1.** Schematic of the modeled glacial-fluvial interface showing feedbacks between the two systems (orange) and the variables altered in our simulations (purple). Panels show the original glacier position (a), glacier advance (b), and glacier retreat (c).

transport, glacial erosion, valley widening, and isostasy. Input parameters include initial grain size, attrition rate, sediment cover, and glaciation (Table 1).

#### 2.1. Bedrock Incision

Fluvial erosion into exposed bedrock is commonly assumed to be proportional to shear stress or stream power (e.g., Howard & Kerby, 1983; Whipple & Tucker, 1999). We use the shear stress derivation of the form:

$$E = R_a k_b \tau_b^a \tag{1}$$

wiley.com/doi/10.1029/2024JF007721 by Colorado College, Wiley Online Library on [03/07/2025]. See the Terms and Conc

where a is a constant equal to 1,  $k_b$  is a constant related to rock properties and erosional process, and  $R_a$  is a sediment buffering term that ranges from 0 (full cover) to 1 (full bedrock exposure). Erosional processes are captured in the constant a (Whipple et al., 2000). Given the complexity of erosion processes and dominance of sediment cover downstream of glaciers (e.g., Anderson & Shean, 2022; Coviello et al., 2022), we chose this simpler stream power/ bedrock exposure model as a general model rather than the more mechanistically specific saltation abrasion model of Sklar and Dietrich (2004). While the exposure model does not allow erosion rates to increase above that calculated by stream power, it does predict lower erosion rates at greater sediment supply and vice versa, which follows the patterns produced by sediment cover and tool effects, respectively. The exposure model is used by previous researchers at similar time and spatial scales (e.g., Hancock & Anderson, 2002; Shobe et al., 2017; Yanites, 2018) and is noted to produce similar results as the full saltation abrasion model (Yanites, 2018) while being much more computationally efficient.

The basal shear stress,  $\tau_b$ , depends on hydraulic radius (R) and slope as follows:

$$\tau_b = \rho gRS \tag{2}$$

$$R = \frac{WH}{2H + W} \tag{3}$$

where  $\rho$  is water density, g is gravitational acceleration, W is channel width, and H is water height for a rectangular shaped channel.

While this approach does not explicitly incorporate the role of sediment as an abrasive tool (Sklar & Dietrich, 2004), the sediment buffer term  $R_a$  modifies E in Equation 1 and is defined by

$$R_a = 1 - Q_s/Q_t \tag{4}$$

where  $Q_s$  is the sediment supply and  $Q_t$  is the total sediment transport capacity in kg. We compared multiple sediment buffer terms (Text S1 in Supporting Information S1) and found they produce similar erosion magnitudes and nearly identical values when erosion and sediment flux are normalized to control simulations.

### 2.2. Sediment Transport

We model the transport of bedload of a median grain size D using the total sediment transport capacity,  $Q_t$  calculated with a modified Meyer-Peter and Müller (1948) equation from Wong and Parker (2006):

$$Q_{t} = 3.97 \rho_{s} W \left[ \frac{\tau_{b}}{(\rho_{s} - \rho)gD} - \tau_{c}^{*} \right]^{\frac{3}{2}} D^{\frac{3}{2}} \sqrt{\frac{\rho_{s} - \rho}{\rho}g}$$
 (5)

SCHANZ AND YANITES 3 of 16

Table	1
Model	Parameters

Model Parameters			
Parameter	Value	Reference	
Fluvial erosion			
Vertical erosivity $k_b$	$-5e-5 \text{ m}^2 \text{ s/kg}$		
Lateral erosivity $k_w$	$-7.3 * k_b$	Finnegan and Dietrich (2011)	
Manning's n	0.04		
Timestep dt	1 year		
Sediment transport			
Shield's parameter $ au_c^*$	0.0495	Wong and Parker (2006)	
Porosity $\lambda$	0.2	Yanites (2018)	
Proportion of eroded hillslope as bedload $\beta$	0.2	Yanites (2018)	
Glacial erosion			
Sliding coefficient, $C_I$	$0.0012 \text{ m}$ $Pa^{-1} \text{ yr}^{-1}$	MacGregor et al. (2000)	
Arrhenius constant, A	$2.1e{-}16 \text{ Pa}^{-3} \text{ yr}^{-1}$	MacGregor et al. (2000)	
Trapezoid angle	30°	MacGregor et al. (2000)	
Maximum width	500 m	MacGregor et al. (2000)	
Mean ELA	2,500 m	Egholm et al. (2009)	
ELA amplitude	1,000 m	Egholm et al. (2009)	
Annual mass balance factor, $\alpha$	0.01 m/(yr-m)	Oerlemans (1984)	
Calculation timestep, $dt_g$	0.1 years		
Isostasy			
Radius of relative stiffness, L	132 km	Pollard and DeConto (2012)	
Flexural rigidity, D	$10^{25}$ N m	Pollard and DeConto (2012)	
Timescale of lithospheric response, <i>τ</i>	3,000 years	Pollard and DeConto (2012)	
Calculation timestep, $dt_i$	10 years		

where  $\rho_s$  is sediment density and  $\tau_c^*$  is Shield's parameter, set at 0.0495 following Wong and Parker (2006). Median bedload size along the model space is assumed to abrade following Sternberg's (1875) law:

$$D = D_0 e^{-a_s x} \tag{6}$$

where  $D_0$  is the initial grain size, x is the downstream distance, and  $a_s$  is the fining parameter or attrition rate. To investigate the effect of sediment size on landscape development, we varied  $D_0$  between 0.01 and 0.5 m and  $a_s$  between 1e-5 and 1e-4 m<sup>-1</sup>. The median grain size is limited to a lower value of 0.0005 m.

Movement of sediment follows mass conservation laws and is modeled using the Exner equation at each node (Exner, 1920, 1925):

$$\frac{\partial h}{\partial t} = -\frac{1}{1 - \lambda_p} \frac{\partial q_s}{\partial x} \tag{7}$$

where  $q_s$  is the sediment flux  $(Q_t - Q_s)$  for each node and  $\lambda_p$  is the bed-sediment porosity. The supply of sediment into each node depends on the transport of sediment from the upstream node  $[Q_s(i-1)]$  as well as the sediment added to the channel through local hillslope transport and tributary flux  $[Q_{Local}(i)]$ . We model the added sediment by assuming a fluvial-hillslope coupling in which the local river channel erosion rates over the last 10 ky drive the local hillslope sediment supply:

$$Q_{Local} = \beta \overline{E} \partial A \tag{8}$$

where  $Q_{Local}$  is the local addition of sediment,  $\beta$  is the proportion of hillslope eroded material that becomes bedload,  $\overline{E}$  is the 10 ky mean erosion rate, and  $\partial A$  is the drainage area added between the previous node and node of interest. All sediment flux out of the last node is allowed to leave the model domain.

#### 2.3. Glacial Erosion

Ice mass balance is calculated following Oerlemans (1984) and MacGregor et al. (2000) in which mass balance linearly increases with initial valley elevation. We use a mass balance gradient ( $\alpha$ ) to calculate the change in ice thickness (b) based on ice elevation ( $z_{ICE}$ ) and equilibrium line altitude (ELA):

$$b = \alpha(z_{ICE} - ELA) \tag{9}$$

but we cap b at 2 m to reflect realistic snow accumulations (e.g., MacGregor et al., 2000). Ice height is then used to calculate shear stress and sliding velocity following the methods of MacGregor et al. (2000). We modify the erosion law to use an erosion rule coefficient of 0.46, which corresponds to glacial quarrying in a heterogeneous bedrock with a Gaussian distribution of fractures from Figure 3 in Iverson (2012):

$$E_q = C_2 U_s^{0.46} (10)$$

where the constant  $C_2$  varies between 0.0001 and 0.0003 (Table 2); this produces annual erosion rates on the order of those calculated for mountain glaciers by Hallet et al. (1996). Based on long-term erosion rates, we use  $C_2 = 0.0002$  for the results presented in this paper (Text S2 in Supporting Information S1). We use a glacier erosion exponent of 0.46; whereas model and field studies suggest that exponents >1 may be more appropriate for individual glacier modeling, particularly for seasonal variations in velocity and erosion (Herman et al., 2018),

SCHANZ AND YANITES 4 of 16

**Table 2** Parameters Used in 800 ky Simulations (n = 180)

Uplift rate (mm/yr)	Initial grain size (m)	Attrition rate (km <sup>-1</sup> )	Glacial erosion constant C2	Glaciation
1	0.5	0.1	0.0001	On
0.5	0.25	0.05	0.0002	Off
0.1	0.1	0.01	0.0003	
	0.05			
	0.01			

exponents <1 are appropriate for mean erosion rates and velocities (Cook et al., 2020).  $U_s$  is the basal sliding velocity, and  $E_q$  is the erosion rate due to quarrying.

We simulate feedbacks between glacial melt, glacial erosion, and fluvial transport by allowing water discharge, sediment flux, and grain size to vary at the first fluvial node (Figure 1). The mass balance of the modeled glacier is tracked, and any meltwater that is generated is added to the discharge of the river downstream. In the case of glacial growth, the glacier advance is assumed to "push" pre-existing sediment downstream, thus increasing the sediment supply. Sediment supply is also enhanced by glacial erosion. Because the glacial erosion law is based on quarrying processes, we assume that all the eroded glacial material becomes bedload; while glacial flour is common in field settings, this results from abrasion, which is not included in the glacial erosion model and is assumed to be dominantly in suspension and thus a minimal contribution to the fluvial bedload. Lastly, bedload sediment attrition (Equation 6) begins at the glacier terminus, allowing the bedload to coarsen with glacier advance (see Text S3 in Supporting Information S1 for sensitivity analysis and further justification of these feedbacks).

#### 2.4. Valley Widening

In glacial settings, valley geometry, and particularly the development of wide valley bottoms, is a key control on sediment storage and glacial erosion. We allow glacial erosion to widen a valley, which in turn decreases the glacier height, leading to decreased glacial erosion rates. The widening valley also provides additional accommodation space for sediment storage.

Glacial erosion widens the valley following the methods in MacGregor et al. (2000) where the initial valley width  $(W_v)$  is equal to the channel width  $(W_v)$ , derived as a function of drainage area (A):

$$W_c = k_c A^b \tag{11}$$

The coefficients  $k_c$  and b are set to 5e-3.5 and 0.5, respectively. The drainage area is calculated from downstream distance (x) using Hack's Law:

$$A = C_h x^{H_e} \tag{12}$$

with coefficients  $C_h = 1$  and  $H_e = 1.8$ . The valley walls are set at an angle of 30° and have a maximum width of 500 m. If vertical glacial erosion is  $E_g$ , then the change in valley width is:

$$\frac{\partial W_{\nu}}{\partial t} = 2E_g \tan(30^{\circ}) \tag{13}$$

As glaciers recede, the widened valleys become sediment storage locations for the river channel, enabling simulation of a paraglacial effect. Sediment is added back to the fluvial system through lateral migration:

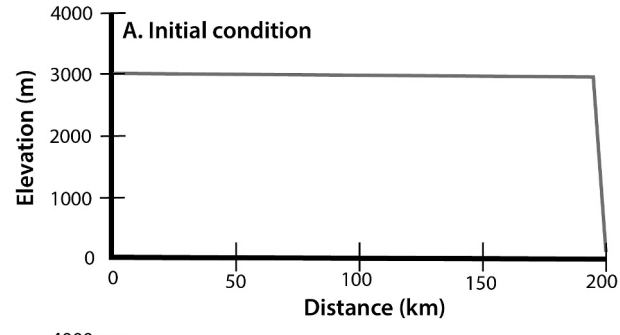
$$Q_{Lat} = k_w \tau_b H \rho_s \partial x \tag{14}$$

where  $Q_{Lat}$  is the lateral sediment supply in kg/s and  $k_w$  is the erosional coefficient that takes into account rock properties and erosional processes. In nodes with prior glaciation, we assume that the banks are alluvial and so  $k_w$ 

SCHANZ AND YANITES 5 of 16

21699011, 2024, 8, Downloaded

.com/doi/10.1029/2024JF007721 by Colorado College, Wiley Online Library on [03/07/2025]. See the Terms



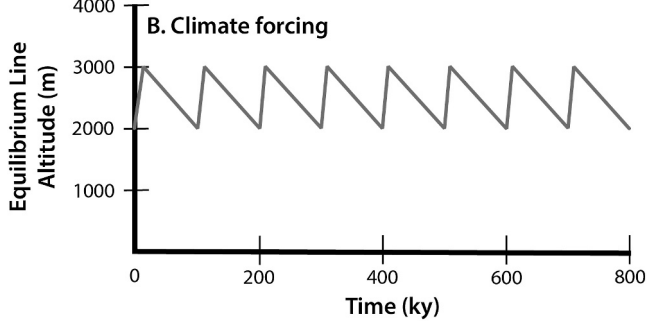


**Figure 2.** (a) Initial model configuration with a 3000-m plateau. (b) Climate forcing during the analysis portion of the simulation.

is set to allow for up to meters per year of lateral erosion for simulated shear stresses. If nodes have not been glaciated, we assume they are bedrock channels and set  $k_w$  for lateral erosion rates of less than mm/yr.

#### 2.5. Isostasy

Isostatic adjustment to erosion is calculated following Huybrechts and de Wolde (1999) and Pollard and DeConto (2012), in which the crustal flexure is a response of asthenospheric relaxation and lithospheric load. The rate of bedrock change  $(\frac{\partial z_i}{\partial t})$  due to loading or unloading is given by:

$$\frac{\partial z_i}{\partial t} = -\frac{1}{\tau} \left( z_b - z_b^{eq} + w_b \right) \tag{15}$$

where  $\tau$  is a response time scale,  $z_b$  is the current bedrock elevation, and  $z_b^{eq}$  is the equilibrium bedrock elevation. The downward deflection  $w_b$  for a given distance r, load P, flexural length scale L, and flexural rigidity D is given by

$$w_b(r) = \frac{PL^2}{2\pi D} kei\left(\frac{r}{L}\right). \tag{16}$$

kei is a kelvin function of zeroth order. Isostatic parameters (Table 1) follow values used by Huybrechts and de Wolde (1999) and Pollard and DeConto (2012).

#### 2.6. Simulations

The model is run for 5 My with only fluvial erosion in order to create a steady-state fluvial profile. To create sufficient initial topography for erosion, we initiate the model as a 3,000 m plateau (Figure 2a) with a fixed end node at 0 m elevation; in all our simulations, this results in a smooth concave up profile at 5 My runtime. After a steady state is achieved, glaciation is imposed with a mean ELA of 2,500 m and a range of 1,000 m following the ELA of Egholm et al. (2009). We then run the model with glaciation for eight 100-ky glacial cycles (Figure 2b). The ELA begins at 2,000 m, then rapidly rises for 10 ky to the maximum 3,000 m, before slowly falling for 90 ky following the sawtooth pattern recorded in both the Vostok ice core and previous coupled glacial-fluvial models (e.g., Braun et al., 1999). While late Cenozoic glaciations have been ongoing for the last 2 My, 800 ky of simulation time allows patterns of topography, erosion rates, and sediment flux to stabilize following the initial glacial adjustment (e.g., Hancock & Anderson, 2002). For each simulation, we also run a control in which glacial erosion is turned off; we refer to this set of simulations as "fluvial-only".

We run the model under varying uplift and sediment conditions (Table 2) in order to understand the controls on glacial extent and landscape modification. Topography, erosion, and sediment flux are saved every 1,000 years to give a timeseries of glacial modification. We ran additional simulations for 3 Ma to compare sediment flux and erosion rates over timescales comparable to late Cenozoic glaciations (Table 3). We do not include the effect of general cooling over the late Cenozoic in the 3 Ma runs as the purpose of this particular modeling exercise is to

**Table 3**Parameters Used in 3 Ma Simulations (n = 10)

Turameters Used in 3 wid simulations $(n-10)$							
Uplift rate (mm/yr)	Initial grain size (m)	Attrition rate (km <sup>-1</sup> )	Glacial erosion constant C2	Glaciation			
0.5	0.5	0.01	0.0002	On			
	0.25			Off			
	0.1						
	0.05						
	0.01						

SCHANZ AND YANITES 6 of 16

21699011, 2024, 8, Downloaded from https://agupubs.onlinelibrary.wiley.com/doi/10.1029/2024JF007721 by Colorado College, Wiley Online Library on [03.07/2025]. See the Terms and Conditions (https://agupubs.onlinelibrary.wiley.com/doi/10.1029/2024JF007721 by Colorado College, Wiley Online Library on [03.07/2025]. See the Terms and Conditions (https://agupubs.onlinelibrary.wiley.com/doi/10.1029/2024JF007721 by Colorado College, Wiley Online Library on [03.07/2025]. See the Terms and Conditions (https://agupubs.onlinelibrary.wiley.com/doi/10.1029/2024JF007721 by Colorado College, Wiley Online Library on [03.07/2025].

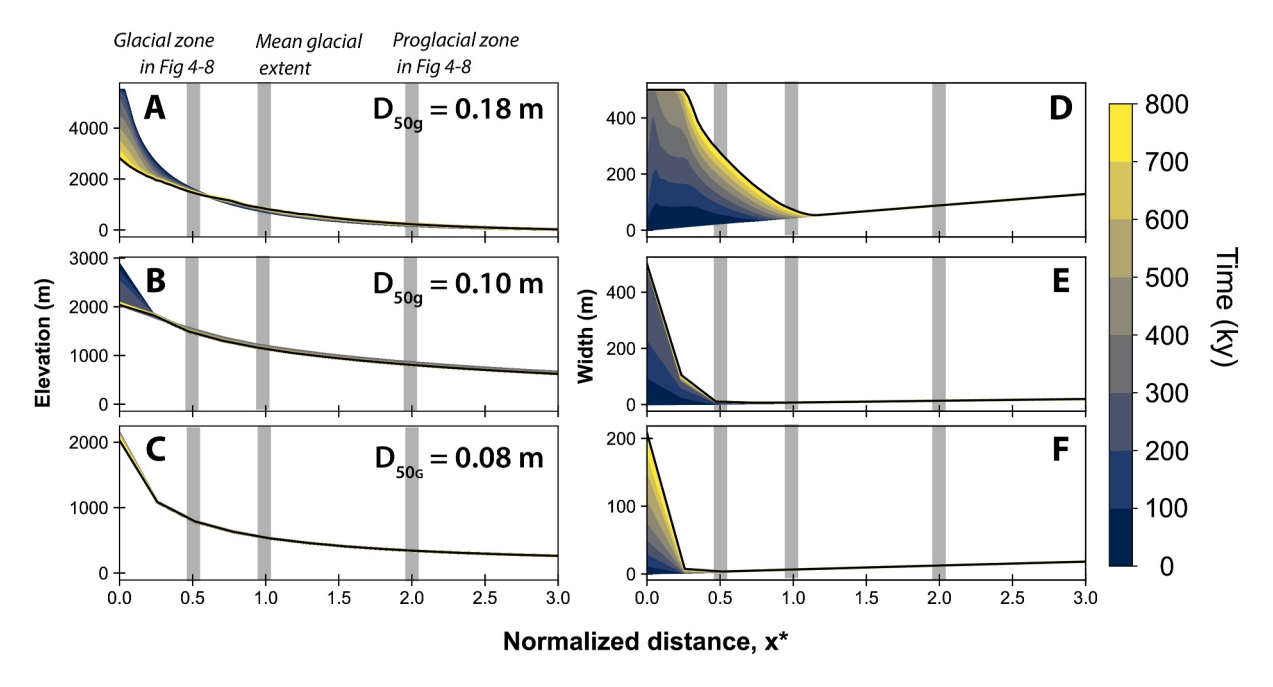


Figure 3. (a–c) Long profile and (d–f) valley width evolution for three simulations with an uplift rate of 0.5 mm/yr; simulations show a range of  $D_{50g}$  values. Gray bars show zones of interest for Figures 4–8. Distance is normalized as  $x^* = \text{distance/mean glacial extent}$  for each simulation.

examine how 800 ky trends continue over a longer timescale rather than replicate rates of erosion and sediment flux in the late Cenozoic.

### 3. Results

## 3.1. Channel Evolution

To compare the effect of glaciation on topographic development, we normalized channel length,  $x^*$ , as channel distance divided by the mean glacial extent of the simulation. Bedrock longitudinal profiles evolve rapidly in response to glaciation with topographic buzzsaw effect and most lateral erosion occurring in the first four glacial cycles (Figure 3). Simulations with initial relief greater than the imposed 2,000–3,000 m ELA experience the most lateral and vertical bedrock erosion and form convexities in the bedrock channel profile where glacial erosion has flattened the channel slope. The profile convexity extends to approximately 2/3 of the mean glacier extent ( $x^* = 0.66$ ) and is formed in the first 200–400 ky as glaciers erode the channel to the lower limit of the ELA. Glacial erosion is initially rapid but slows considerably as the topography reaches a buzzsaw elevation.

While glaciation results in rapid bedrock erosion down to a topographic buzzsaw level, the bedrock channel downstream of the glacier undergoes surface uplift on the order of meters to tens of meters (Figures 3a and 3b). Although this is much lower in magnitude than the >1,000 m of erosion in the glaciated reach, surface uplift occurs over a zone of 30 km, indicating that bedrock erosion is not keeping pace with rock uplift.

To further investigate the trends in glacial and proglacial erosion, we define two zones for further analysis: a glacial zone at half the mean glacial extent ( $x^* = 0.5$ ) and a proglacial zone at two times the mean glacial extent ( $x^* = 2$ ). This allows us to compare similar erosion processes across simulations with a wide range of glacial extents. Additionally, we compare the effect of the initial grain size and attrition rate by differentiating simulations based on the median grain size in the glacial zone ( $D_{500}$ ).

Sediment depth patterns imitate the long profile evolution trends and suggest that sediment has modulated erosion rates downstream of the glaciated zone (Figure 4). In the glacial zone, sediment aggradation behaves differently for simulations with  $D_{50g}$  of less than and greater than 0.1 m. At larger  $D_{50g}$  values, aggradation occurs during interglacial periods but is transported downstream during glacial occupation (Figure 4a). Interglacial aggradation is caused by lowered slopes due to the intense glacial erosion, which lowers the transport capacity in the glaciated reaches (Figure 3) and results in sediment accumulation. The highest accumulation tends to occur between the

SCHANZ AND YANITES 7 of 16

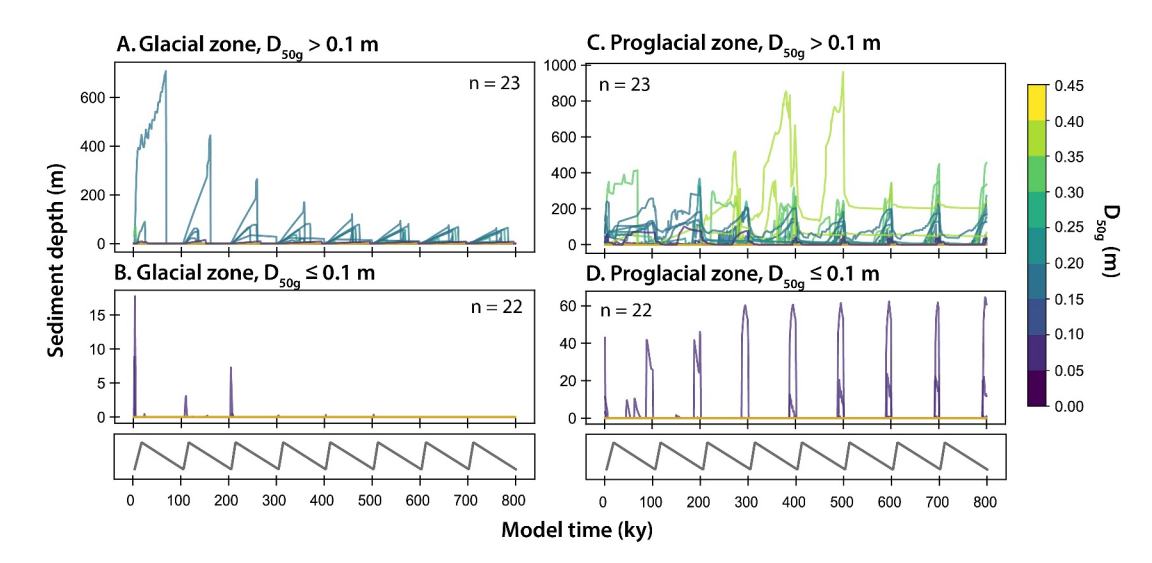


Figure 4. Sediment depth through the model simulations at (a, b) glaciated zone ( $x^* = 0.5$ ) and (c, d) proglacial zone ( $x^* = 2$ ). Lines are colored by the  $D_{50g}$  value and separated into  $D_{50g} > 0.1$  m (a, c) and <0.1 m (b, d). Orange lines represent simulations that did not have sufficient topography to form glaciers. Bottom panels show the imposed ELA (Figure 2 for values).

first and fourth glacial cycles, corresponding to when glacial erosion forms a buzzsaw-determined elevation profile (Figure 3). In contrast, simulations with smaller  $D_{50g}$  values tend to show either no sediment aggradation or short-lived aggradation during deglaciation, though aggradation becomes negligible after the third glacial cycle (Figure 4b).

In contrast, sediment depths are much greater and in an opposite pattern in the proglacial zone (Figures 4c and 4d). Sediment is deposited in cycles that correspond to the maximum glacial period, and reaches consistent depths of 50 m, with maxima of 900 m for simulations with the largest  $D_{50g}$ . During interglacial periods, the sediment is transported away, and in all but three simulations, the channel returns to bare bedrock. Unlike sediment in the glacial zone, aggradation patterns are similar for all  $D_{50g}$  values in glaciated simulations. However, this cyclic aggradation pattern is not immediately established; most simulations take four glacial cycles to reach a recurring pattern with consistent aggradation depths. This timescale is consistent with the buzzsaw response and valley width adjustment timescales (Figure 3) and with simulations of river terrace formation in response to glacial cycles (Hancock & Anderson, 2002).

Sediment depths in the proglacial zone are thick enough to act as a significant erosion cover and are the cause of overall surface uplift (Figures 3a and 3b) produced by damped bedrock erosion rates that do not keep pace with rock uplift. Sensitivity analyses (Figure S3 in Supporting Information S1) show that sediment aggradation results from the increase in bedload grain size due to glacier advance; therefore, this surface uplift—and damping of bedrock erosion—is directly caused by glaciation. However, based on the topographic profile, it is unclear whether the surface uplift is of a magnitude needed to balance the rapid bedrock erosion in the glacial zone. In the next sections, we analyze bedrock erosion rates in the glacial and proglacial zones and contrast these to steady-state erosion rates.

#### 3.2. Bedrock Erosion Rates

To compare erosion values across simulations, we normalized erosion rates,  $E^*$ , as erosion rates in glacial simulations divided by erosion rates in fluvial-only simulations. High erosion rates are expected in the glacial zone where glacial erosion limits topography (buzzsaw effect) (Figure 3). For simulations undergoing glaciation, calculated erosion rates initially increase to up to 25–50 m/ky greater than erosion rates in fluvial-only simulations (Figure 5a). Initial landscape lowering is dependent on grain size; when the  $D_{50g}$  value of the glacial zone is larger than 0.1 m, erosion rates are >5 times the fluvial-only erosion rates (Figure 5a) in contrast to smaller  $D_{50g}$  values in which erosion rates are within an order of magnitude of the fluvial-only rates.

SCHANZ AND YANITES 8 of 16

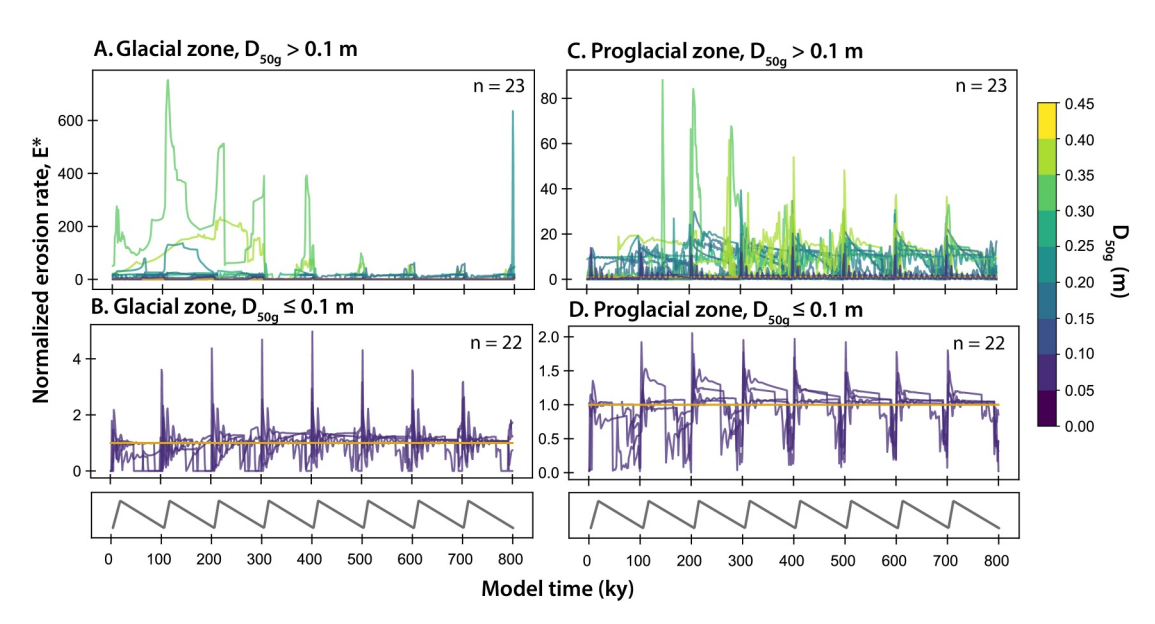


**Figure 5.** Normalized bedrock erosion rate at the glacial zone ( $x^* = 0.5$ ) shown in panels (a, b) and in the proglacial zone ( $x^* = 2$ ) in panels (c) and (d). Erosion rates vary by  $D_{50g}$  and are split into  $D_{50g} > 0.10$  m (panels a and c) and  $D_{50g} < 0.10$  m (panels b and d). Orange lines indicate runs with insufficient relief to generate glaciation. Normalized erosion rate, E\*, is glacial erosion rate/fluvial-only erosion rate. Bottom panels show the imposed ELA (Figure 2 for values).

High bedrock erosion rates are not sustained; by 400 ky, all simulations have settled into a pattern wherein interglacial erosion rates are the same or lower than fluvial-only simulations but increase up to 5–20x fluvial steady-state rates during the glacial period (Figures 5a and 5b). Simulations with smaller  $D_{50g}$  tend to have a sharp increase in erosion rates at peak glaciation, then a damped erosion signal as material is transported downstream in the early interglacial (Figure 5b). In contrast, higher  $D_{50g}$  simulations, which tend to have higher relief, have heightened bedrock erosion rates in the early and mid-glacial periods. This difference is due to the relief within each simulation; simulations with  $D_{50g}$  values less than 0.1 m have a buzzsawed relief that does not produce glaciation until the lowest imposed ELA.

In the proglacial zone downstream of the simulated glaciers, erosion rates are dictated by fluvial processes but are subject to high-frequency changes in sediment transport capacity and flux—which drives variations in bedrock erosion via reduced cover (Sklar & Dietrich, 2001)—from upstream glaciers. During the first 400 ky, the glacial buzzsaw effect and associated sediment production cause variable bedrock erosion rates, as each simulation erodes from a unique spin-up fluvial profile (Figures 5c and 5d). After 400 ky, bedrock erosion rates begin to follow a cyclic pattern with a spike in erosion rates up to 20 times greater than fluvial-only erosion rates immediately post-glaciation, followed by a decrease to just 2%–5% of the nonglacial erosion rate. Simulations with  $D_{50g} > 0.35$  m take up to 500 ky to achieve this pattern. Erosion rates continue to fluctuate between high and low values with a damped oscillation throughout the interglacial period. These patterns of bedrock erosion in the proglacial zone are a result of sediment aggradation and transport controlled by the increase in bedload size caused by glacier advance (Figure S3 in Supporting Information S1).

#### 3.2.1. Averaged Bedrock Erosion Rates

Glaciation causes short-lived changes in erosion rates in the glacial and proglacial zones, but long-term averaged erosion rates are damped as more of the interglacial period is incorporated. We calculated erosion rates over different timescales, starting from the end of the simulation up to the onset of glaciation at 800 ky. For instance, an averaging time of 10 ky uses erosion rates from 790 to 800 ky in the simulation and is representative of field-based erosion rates measured from a 10 ky rock or sediment sample. We also ran a subset of models that resulted in a range of glacial extents for 3 Ma (Table 3).

In the glacial zone, time-averaged erosion rates are initially similar or higher than fluvial-only erosion rates (Figures 6a and 6b) because the model ends in a glacial period. The high averaged erosion rates are consistent with the high erosion rates at 800 ky in Figures 5a and 5b. Averaged erosion rates steadily decline as an

SCHANZ AND YANITES 9 of 16

21699011, 2024, 8, Downloaded from https://agupubs.onlinelibrary.wiley.com/doi/10.1029/2024JF007721 by Colorado College, Wiley Online Library on [03:07/2025]. See the Terms

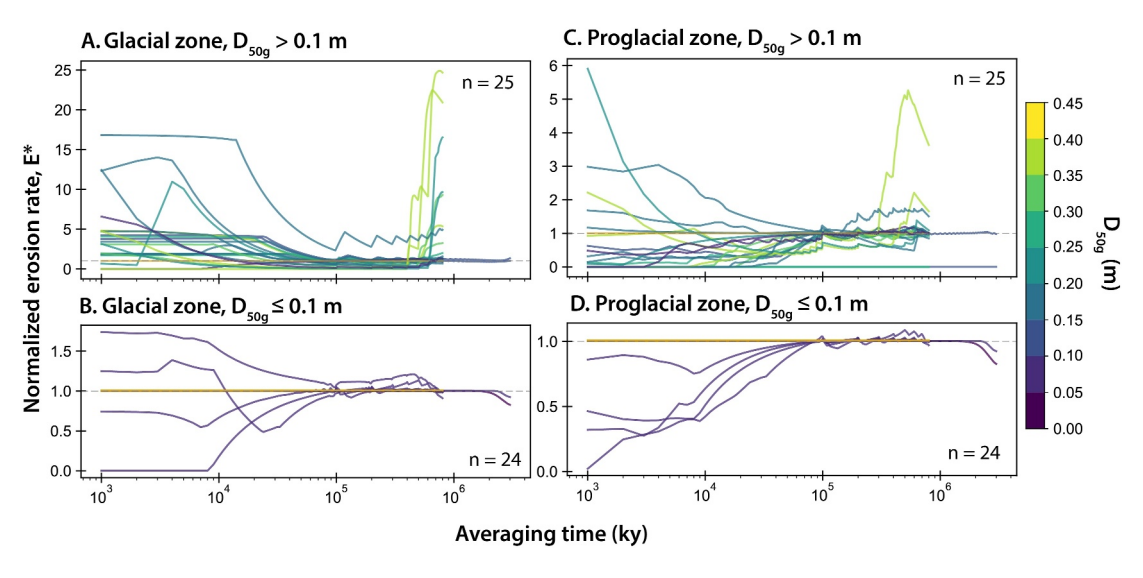


Figure 6. Normalized time-averaged erosion rates at (a, b) glacial zone ( $x^* = 0.5$ ) and (c, d) proglacial zone ( $x^* = 2$ ). Simulations are split into  $D_{50g} > 0.1$  m (a, c) and  $D_{50g} < 0.1$  m (b, d). The averaging time is relative to the end of simulations (800 ky in Figure 4 or 3 My for long runs). Orange lines represent simulations in which initial relief was too low to generate glaciers.

interglacial period and the associated low erosion rates are integrated. At 100 ky averaging time, averaged erosion rates increase slightly because the 700 ky glacial period is integrated. Averaged erosion rates approach fluvial-only values as more glacial cycles are integrated and proportionally more of the averaging time is spent in interglacial periods. However, for simulations with  $D_{50g}$  values above 0.2 m, averaged erosion rates rise rapidly when the onset of glaciation is integrated and can be up to 25 times larger than fluvial-only erosion rates. Because the initial topography and relief are greater with larger grain sizes, the initially high erosion rates corresponding with the topographic buzzsaw are also dependent on grain size properties (Figure 5a) and thus the 800 ky averaged rates are sensitive to grain size (Figure 6a). However, when glaciation has been ongoing for 3 Ma, similar to timescales of periodic alpine glaciation, averaged erosion rates are at maximum only 2–3 times greater than the fluvial-only control.

In the proglacial zone, erosion rates are more variable over time (Figures 5c and 5d), yet the time averaged erosion rates converge for simulations with  $D_{50g}$  values <0.1 m (Figures 6c and 6d). Averaged erosion rates are initially lower than the fluvial steady state, particularly for short averaging times in which glacial states predominate. Glacial periods result in aggradation in the proglacial zone and minimal bedrock erosion. As the averaging time increases toward  $10^5$  years and incorporates the interglacial period, the averaged erosion rate approaches a steady state. By the time 800 ky is integrated into the averaged erosion rate, including achievement of a topographic buzzsaw and onset of glaciation, averaged erosion rates for simulations with  $D_{50g}$  values <0.1 m are within 90%–110% of the steady state. This implies that the fluvial zone downstream of glaciers may experience damped erosion rates at timescales of <100 ky, but rapid erosion rates in the post-glacial period (Figures 5c and 5d) compensate for the lowered erosion rates during the late interglacial and glacial periods and approximate rock-uplift rates at >100 ky timescales.

#### 3.3. Sediment Flux

Glacial advance and retreat alter the sediment size distribution and cause aggradation and erosion; consequently, the sediment exported out of the system into downstream basins must be temporally variable with glacial cycles. We examine the sediment flux, defined as the sediment leaving the last node of the model, over the 800 ky model runtime and normalize the sediment flux against the sediment flux in fluvial-only simulations with the same sediment and uplift parameters. This normalization is used because we found that sediment flux values are sensitive to the choice of bedrock erosion model, but that the ratio of glacial to fluvial-only sediment fluxes was relatively insensitive to the erosion model choice (Figure S1 in Supporting Information S1).

Sediment flux out of the model initially has a cyclic nature that is most pronounced for simulations with  $D_{50g}$  values >0.1 m (Figure 7a). For these larger grain sizes, sediment flux is lower than fluvial-only simulations for

SCHANZ AND YANITES 10 of 16

21699011, 2024, 8, Downloaded from https://agupubs.onlinelibrary.wiley.com/doi/10.1029/2024JF007721 by Colorado College, Wiley Online Library on [03/07/2025]. See the Terms and Condit

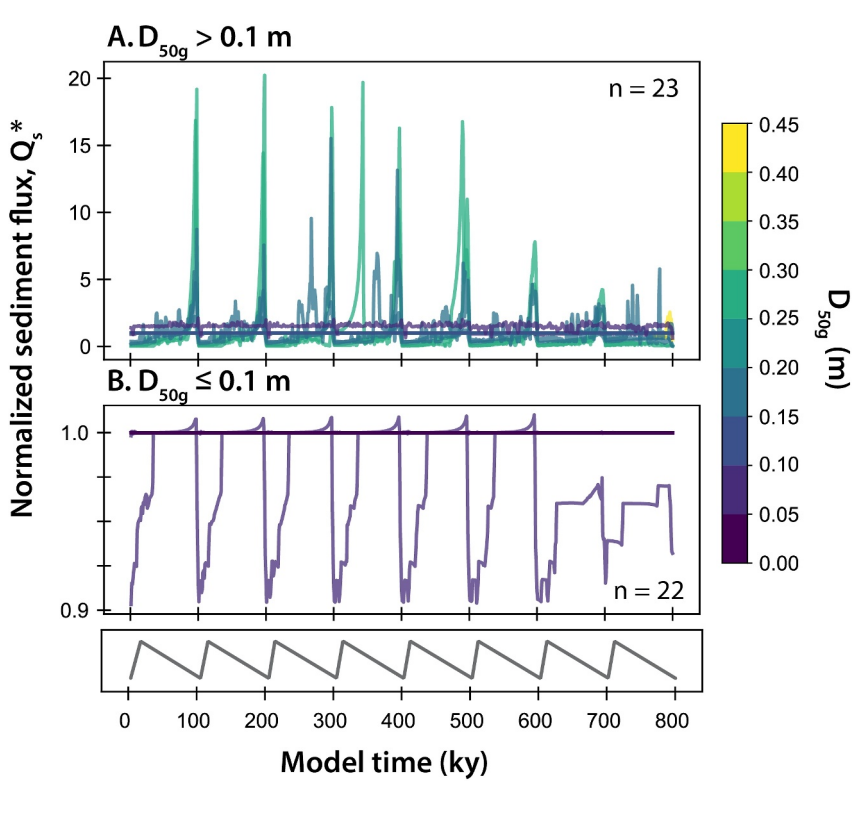


**Figure 7.** Sediment flux out of the simulations shown over model time and separated by the median grain size in the glacial zone ( $D_{50g}$ ). Normalized sediment flux,  $Q_{8}$ \*, is defined as sediment flux from the glacial simulation divided by the fluvial-only simulation flux. The bottom panel shows the imposed ELA (Figure 2 for values).

most of the model period but increases during the early glacial period. Most simulations, however, are within 90%–110% of the nonglacial sediment flux values, particularly for  $D_{50g}$  less than 0.1 m (Figure 7b). The pattern of sediment flux out over a glacial cycle is similar to the pattern of proglacial aggradation but opposite to the aggradation pattern in the glacial zone (Figure 4). This suggests that the glacial zone, with the wider valleys (Figures 3d–3f), is a location of sediment storage during the interglacial period but a source of sediment for proglacial aggradation and sediment flux out of the model during the glacial period.

Simulations with larger  $D_{50g}$  values have more pronounced variability in sediment flux because these simulations are associated with greater glacial extents. Glacier extent controls the initial grain size distribution and thus the sediment transport capacity during glaciation. Interestingly, normalized sediment flux patterns are similar during and after the buzzsaw erosion adjustment period, further supporting that sediment flux is more strongly controlled by glacial alteration to grain size than by increases in sediment supply from glacial erosion.

Time averaged sediment fluxes, with the exception of three simulations, are lower or similar to fluvial-only fluxes due to the decreased sediment fluxes in the early to middle interglacial periods (Figure 8). At short averaging periods of <100 ky, averaged sediment fluxes ranged from 2% to 90% of the fluvial-only values. As the early interglacial and corresponding high sediment flux are incorporated at 100 ky averaging periods, the averaged sediment flux rapidly increases to within 10% of the fluvial-only value. By an averaging time of 800 ky, averaged sediment fluxes for the majority of simulations are 90%–100% of nonglacial values and thus are nearly indistinguishable. The exceptions to this trend are simulations with high (>0.1 m)  $D_{50g}$  values (Figure 8a) in which >25% of the model domain is glaciated. These simulations give sediment fluxes within 50%–150% of nonglacial values and suggest that basin accumulation rates reflect glaciation if >25% of the contributing basin is glaciated. However, the average sediment flux trend in Figure 8a shows that these values may be approaching the fluvial-only flux values at timescales >800 ky and notably do not approach the >500% increase in bedrock erosion rates noted in the glacial zone (Figure 6).

SCHANZ AND YANITES 11 of 16

21699011, 2024, 8, Downloaded from https://agupubs.onlinelibrary.wiley.com/doi/10.1029/2024JF007721 by Colorado College, Wiley Online Library on [03/07/2025]. See the Terms

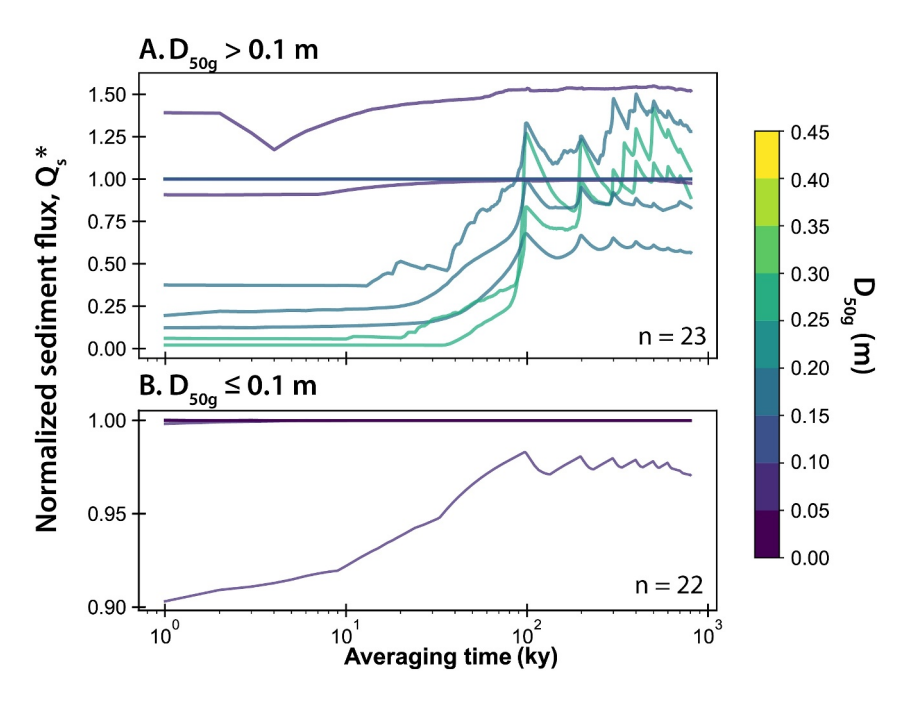


Figure 8. Time-averaged sediment flux is shown for two  $D_{50g}$  grain size ranges. Normalized sediment flux is defined as glacial simulation sediment flux divided by fluvial-only simulation sediment flux. Averaging time is referenced to present, or year 800 ky of the model.

#### 4. Discussion

We find that damping of bedrock erosion from the transport and storage of glacially derived sediment results in landscape-scale sediment fluxes that are indistinguishable from unglaciated landscapes. A key disconnect in the late Cenozoic erosion debate is that erosion rates increase locally, particularly in high elevations (Herman et al., 2013), while sediment fluxes to basins give conflicting results with some evidence for steady accumulation rates (Sadler & Jerolmack, 2015; Willenbring & von Blanckenburg, 2010) and other evidence supporting a rapid increase in accumulation rates in the late Cenozoic (Hay et al., 1988; Molnar, 2004). By incorporating sediment cover effects and feedbacks between glacial position and transport capacity, our model replicates both the 2- to 4-fold increase in bedrock erosion rates (Figure 6), as well as the steady sedimentation rates (Figure 8); we thus offer a potential mechanism to reconcile the disparity between point- and basin-wide erosion measurements.

This finding is supported by spatially localized evidence for (a) rapid and efficient bedrock erosion in the glaciated reach, (b) lowered erosion rates in the proglacial zone, and (c) temporally unsteady sediment fluxes out of the model. Below, we compare the numerical results in glaciated, proglacial, and outlet localities with observational data to show how our numerical model produces results consistent with prior work and gives higher temporal resolution to erosion trends.

Prior studies have documented rapid and efficacious glacial bedrock erosion over different timescales. At the scale of months, Herman et al. (2015) measured erosion rates up to 50 times greater than background uplift rates that range from 1 to 500 mm/yr. Qualitatively, Kirkbride and Matthews (1997) used space-for-time analysis to find that glacial landforms in New Zealand are carved in the first 200 ky of glaciation, whereas Shuster et al. (2005) quantified glacial erosion rates at the 10<sup>6</sup> timescale and found that glacial erosion removed 1.7–2.2 km of rock in the first 400 ky, with only 0.3 km removed in the subsequent 1.4 Ma in the Coast Range of British Columbia, Canada. Literature compilations reveal a negative correlation between measurement interval and erosion rate: Koppes and Hallet (2006) found that erosion rates increased 3.5 times going from 10<sup>5</sup> to 10<sup>1</sup> timescales, and in a compilation of erosion rates in glaciated landscapes, Ganti et al. (2016) show that erosion rates generally display a two-order-of-magnitude decrease from 10 years to 10 My, with a negative power law relationship between averaging time and erosion rate.

SCHANZ AND YANITES 12 of 16

However, these data sets are drawn from erosion measurements that differ in collection method, timescale, and, importantly, location. Through use of a numerical model, we are able to compare similar data across the same simulated glacial conditions, and thereby make a more direct comparison. Notably, our erosion rates are consistent with the field measurements; short term erosion rates are up to 100 times background uplift rates (Figure 5), glacial buzzsaw topography forms within 400 ky (Figure 3), and erosion rates computed at different timescales show a power law decrease consistent with the compilation data (Ganti et al., 2016; Koppes & Hallet, 2006). Our data matching field and literature compilations suggests that the power law decrease in erosion rate with averaging time cannot be explained by differences in erosion rate method, timescale, or location but must be intrinsic to landscape evolution under glacial erosion processes. Additionally, the agreement in erosion rate trends between our model—in which the glacial erosion coefficient C2 is calibrated to tectonically active areas—and global compilations suggests that the trends and patterns we find are likely applicable in less tectonically active regions.

We found that decreased bedrock erosion rates in the proglacial zone result from aggradation of a coarser bedload during glaciation that is then transported during the interglacial. Although our 1-D model cannot capture changes in sediment flux and erosion caused by hillslope dynamics, periglacial processes, and lateral channel migration—thus limiting our analysis of proglacial aggradation—the patterns of erosion and aggradation are consistent with field observations. Proglacial erosion and aggradation histories are recorded in bedrock terraces, which are frequently planed during glacial periods—indicating sediment aggradation that inhibits bedrock incision—and incised during post-glacial or interglacial periods (e.g., Hancock & Anderson, 2002; Schanz et al., 2018). This chronology matches our modeled proglacial aggradation patterns (Figures 5c and 5d). Proglacial erosion rate patterns are similar to those noted by Malatesta et al. (2018) in the Tian Shan of central Asia, in which bedrock erosion rates reach a maxima 6–16 ka after glaciation when aggraded sediment has been removed.

Calculated sediment flux out of our model decreased during glaciation and increased during the early interglacial because of glacially driven increases in grain size and corresponding decreases in sediment transport capacity (Equation 5). This can be compared with flux predictions from the paraglacial model of Church and Ryder (1972), which predicts fluvial aggradation during deglaciation followed by incision as deglaciation ends. Field data taken along the Thompson River, British Columbia, shows aggradation thicknesses of the order of 175 m and accumulate in 1 ky of deglaciation, with incision into those deposits in the following 10 ky (Church & Ryder, 1972). The paraglacial model would thus predict low sediment fluxes out of the fluvial system during deglaciation when sediment—particularly bedload—is aggrading, followed by high sediment fluxes as the aggraded material is remobilized in the following 10 ky. This pattern is consistent with our model results. Additionally, higher sediment fluxes associated with glacial retreat have been noted in the Patagonian Andes (Koppes et al., 2015) and the Canadian Rocky Mountains (Leonard, 1997) for Holocene neoglacial activity.

The agreement between our spatially localized findings and prior field observations for glacial erosion, proglacial erosion, and outlet sediment flux lends strength to our modeling approach, despite the limitations of a one-dimensional model, and suggests that our main finding—that transport and storage of glacially derived bedload can slow basin-wide erosion rates and damp sediment fluxes—is robust.

We emphasize that the patterns of erosion and transport are transferrable, but note that future work is necessary to compare rates. In particular, our model lacks sediment transport and storage in the glacial regime and does not explicitly include a tool effect in bedrock erosion, which could allow erosion rates to increase above that predicted by the shear stress model. Inclusion of these factors would allow workers to more directly compare measured erosion rates with those predicted by the model. Additional work could also test the effect of a general cooling trend over the late Cenozoic on glacial and proglacial erosion trends and use direct temperature records to control the ELA rather than a cyclic seesaw pattern.

An implication of these results is that the reduction in erosion rate and subsequent surface uplift in proglacial reaches can continue to feed glacial erosion, facilitating a glacial landscape steady state. Numerical modeling of glacial erosion reveals a tendency of cryocide, where the efficient erosion of glaciers lowers topography below the ELA, resulting in diminishing glacial extent (Anderson et al., 2012). However, the surface uplift resulting from the reduction in fluvial erosion efficiency acts as a potential feedback to continue feeding the glaciated part of the landscape new rock to maintain erosion rates without reducing the glacial length. This supports numerical modeling observations showing that glacial extent is sensitive to the basin hypsometry developed in prior glaciations (Pedersen & Egholm, 2013).

SCHANZ AND YANITES 13 of 16

Acknowledgments

anonymous reviewer.

Funding was provided by NSF EAR

draft. This manuscript benefited

Anderson, George Hilley, and an

substantially from feedback by Bob

2120210 (SS) and 2120211 (BY). Thanks

to Paul Myrow for reviewing an earlier

This finding adds to a growing body of conceptual and numerical models that stress the importance of sediment transport and erosion in glacially altered landscapes. Under glaciers, sediment transforms the drag at the ice-bed interface, and new slip laws seek to better parameterize basal sediment to understand ice sheet movement (Zoet & Iverson, 2020). At the glacier-fluvial interface, temporal changes in sediment availability and connectivity under a glacier system create cyclical variations in sediment yield (Antoniazza & Lane, 2021), and feedbacks between glacially sculpted overdeepenings and sediment transfer can drive short-term, but high-volume, transfers of sediment (Swift et al., 2018). Topography created by glacial deposition and erosion alters the rates and timing of fluvial sediment transfer in post-glacial periods (Lane et al., 2017). Our model also stresses the importance of glacially derived bedload in altering fluvial erosion and sediment fluxes, thus emphasizing the need to better understand and account for sediment dynamics, particularly when upscaling point-measurements of erosion and deposition to basin- or continental-integrated measurements. Future studies on alpine landscape evolution should incorporate the armoring effect of glacially produced sediment on downstream fluvial systems.

## 5. Conclusions

Using a 1-D finite difference model, we simulated the development of topography and sediment flux under glacial and fluvial erosion. The dependence of sediment transport capacity on glacial cycles, particularly the dependence of bedload size on glacier extent, leads to cyclic changes in aggradation, erosion rate, and sediment fluxes throughout a 200 km-long model, even though glaciers on average only occupy the upper 6–8 km. In the proglacial zone, sediment aggradation decreases bedrock erosion rates below those simulated for unglaciated rivers with the same uplift and sediment characteristics; this aggradation-driven damping of bedrock erosion provides a basin-wide balance to the increase in bedrock erosion rates in glaciated reaches. Sediment flux out of the model is steady at timescales >100 ky and matches nonglacial fluxes. By incorporating sediment dynamics into the model, erosion rates and sediment fluxes match patterns in alpine valleys and ocean basins, respectively. We propose that glacially derived bedload is the missing ingredient that can reconcile Late Cenozoic measurements of erosion and sediment flux and stress the importance of sediment dynamics when extending point measurements to the landscape scale.

### **Data Availability Statement**

The Python model used to simulate glacial and fluvial erosion is hosted on Github (Schanz, 2024). Version 1.0.0 contains the scripts used to produce Figures 3–8. All model results are publicly available on Zenodo (Schanz & Yanites, 2024).

#### References

Anderson, R. S., Dühnforth, M., Colgan, W., & Anderson, L. (2012). Far-flung moraines: Exploring the feedback of glacial erosion on the evolution of glacier length. Geomorphology, 179, 269–285. https://doi.org/10.1016/j.geomorph.2012.08.018

Anderson, S. W., & Shean, D. (2022). Spatial and temporal controls on proglacial erosion rates: A comparison of four basins on Mount Rainier, 1960 to 2017. Earth Surface Processes and Landforms, 47(2), 596–617. https://doi.org/10.1002/esp.5274

Antoniazza, G., & Lane, S. N. (2021). Sediment yield over glacial cycles: A conceptual model. *Progress in Physical Geography: Earth and Environment*, 45(6), 842–865. https://doi.org/10.1177/0309133321997292

Berger, A. L., & Spotila, J. A. (2008). Denudation and deformation in a glaciated orogenic wedge: The St. Elias orogen, Alaska. *Geology*, 36(7), 523–526. https://doi.org/10.1130/G24883A.1

Boulton, G. S. (1978). Boulder shapes and grain-size distributions of debris as indicators of transport paths through a glacier and till genesis. Sedimentology, 25(6), 773–799. https://doi.org/10.1111/j.1365-3091.1978.tb00329.x

Braun, J., Zwartz, D., & Tomkin, J. H. (1999). A new surface-processes model combining glacial and fluvial erosion. *Annals of Glaciology*, 28, 282–290. https://doi.org/10.3189/172756499781821797

Brocklehurst, S. H., & Whipple, K. X. (2002). Glacial erosion and relief production in the Eastern Sierra Nevada, California. *Geomorphology*, 42(1–2), 1–24. https://doi.org/10.1016/S0169-555X(01)00069-1

Brozović, N., Burbank, D. W., & Meigs, A. J. (1997). Climatic limits on landscape development in the Northwestern Himalaya. *Science*, 276(5312), 571–574. https://doi.org/10.1126/science.276.5312.571

Campforts, B., Shobe, C. M., Steer, P., Vanmaercke, M., Lague, D., & Braun, J. (2020). HyLands 1.0: A hybrid landscape evolution model to simulate the impact of landslides and landslide-derived sediment on landscape evolution. *Geoscientific Model Development*, 13(9), 3863–3886. https://doi.org/10.5194/gmd-13-3863-2020

Church, M., & Ryder, J. M. (1972). Paraglacial sedimentation: A consideration of fluvial processes conditioned by glaciation. *Geological Society of America Bulletin*, 83(10), 3059. https://doi.org/10.1130/0016-7606(1972)83[3059:PSACOF]2.0.CO;2

Comiti, F., Mao, L., Penna, D., Dell'Agnese, A., Engel, M., Rathburn, S., & Cavalli, M. (2019). Glacier melt runoff controls bedload transport in Alpine catchments. Earth and Planetary Science Letters, 520, 77–86. https://doi.org/10.1016/j.epsl.2019.05.031

Cook, S. J., Swift, D. A., Kirkbride, M. P., Knight, P. G., & Waller, R. I. (2020). The empirical basis for modelling glacial erosion rates. *Nature Communications*, 11(1), 759. https://doi.org/10.1038/s41467-020-14583-8

SCHANZ AND YANITES 14 of 16

- Coviello, V., Vignoli, G., Simoni, S., Bertoldi, W., Engel, M., Buter, A., et al. (2022). Bedload fluxes in a glacier-fed river at multiple temporal scales. Water Resources Research, 58(10), e2021WR031873. https://doi.org/10.1029/2021WR031873
- Cowie, P. A., Whittaker, A. C., Attal, M., Roberts, G., Tucker, G. E., & Ganas, A. (2008). New constraints on sediment-flux-dependent river incision: Implications for extracting tectonic signals from river profiles. *Geology*, 36(7), 535–538. https://doi.org/10.1130/G24681A.1
- Egholm, D. L., Nielsen, S. B., Pedersen, V. K., & Lesemann, J.-E. (2009). Glacial effects limiting mountain height. *Nature*, 460(7257), 884–887. https://doi.org/10.1038/nature08263
- Exner, F. M. (1920). Zur physik der dünen. Hölder.
- Exner, F. M. (1925). Uber die wechselwirkung zwischen wasser und geschiebe in flussen, Akad. der Wiss in Wien, Math-Naturwissenschafliche Klasse, Sitzungsberichte. Abt Ila, 134, 165–203.
- Finnegan, N. J., & Dietrich, W. E. (2011). Episodic bedrock strath terrace formation due to meander migration and cutoff. *Geology*, 39(2), 143–146. https://doi.org/10.1130/G31716.1
- Ganti, V., von Hagke, C., Scherler, D., Lamb, M. P., Fischer, W. W., & Avouac, J.-P. (2016). Time scale bias in erosion rates of glaciated landscapes. *Science Advances*, 2(10), e1600204. https://doi.org/10.1126/sciadv.1600204
- Hallet, B., Hunter, L., & Bogen, J. (1996). Rates of erosion and sediment evacuation by glaciers: A review of field data and their implications. Glob. Planet. Change, Impact of Glaciations on Basin Evolution: Data and Models from the Norwegian Margin and Adjacent Areas, 12(1-4), 213–235. https://doi.org/10.1016/0921-8181(95)00021-6
- Hammer, K. M., & Smith, N. D. (2008). Sediment production and transport in a proglacial stream: Hilda Glacier, Alberta, Canada. *Boreas*, 12(2), 91–106. https://doi.org/10.1111/j.1502-3885.1983.tb00441.x
- Hancock, G. S., & Anderson, R. S. (2002). Numerical modeling of fluvial strath-terrace formation in response to oscillating climate. Geological Society of America Bulletin, 114(9), 1131–1142. https://doi.org/10.1130/0016-7606(2002)114<1131:NMOFST>2.0.CO;2
- Hay, W. W., Sloan, J. L., & Wold, C. N. (1988). Mass/age distribution and composition of sediments on the ocean floor and the global rate of sediment subduction. *Journal of Geophysical Research*, 93(B12), 14933–14940. https://doi.org/10.1029/JB093iB12p14933
- Herman, F., Beyssac, O., Brughelli, M., Lane, S. N., Leprince, S., Adatte, T., et al. (2015). Erosion by an Alpine glacier. *Science*, 350(6257), 193–195. https://doi.org/10.1126/science.aab2386
- Herman, F., Braun, J., Deal, E., & Prasicek, G. (2018). The response time of glacial erosion. *Journal of Geophysical Research: Earth Surface*, 123(4), 801–817. https://doi.org/10.1002/2017JF004586
- Herman, F., Seward, D., Valla, P. G., Carter, A., Kohn, B., Willett, S. D., & Ehlers, T. A. (2013). Worldwide acceleration of mountain erosion
- under a cooling climate. Nature, 504(7480), 423–426. https://doi.org/10.1038/nature12877
  Howard, A. D., & Kerby, G. (1983). Channel changes in badlands. Geological Society of America Bulletin, 94(6), 739–752. https://doi.org/10.1038/nature12877
- 1130/0016-7606(1983)94<739:CCIB>2.0.CO;2
  Huybrechts, P., & de Wolde, J. (1999). The dynamic response of the Greenland and Antarctic Ice Sheets to multiple-century climatic warming.
- Journal of Climate, 12(8), 2169–2188. https://doi.org/10.1175/1520-0442(1999)012<2169:TDROTG>2.0.CO;2
- Iverson, N. R. (2012). A theory of glacial quarrying for landscape evolution models. Geology, 40(8), 679–682. https://doi.org/10.1130/G33079.1
  Kirkbride, M., & Matthews, D. (1997). The role of fluvial and glacial erosion in landscape evolution: The Ben Ohau Range, New Zealand. Earth Surface Processes and Landforms, 22(3), 317–327. https://doi.org/10.1002/(SICI)1096-9837(199703)22:3<317::AID-ESP760>3.0.CO;2-I
- Koppes, M., & Hallet, B. (2006). Erosion rates during rapid deglaciation in Icy Bay, Alaska. J. Geophys. Res. Earth Surface, 111(F2). https://doi.org/10.1029/2005JF000349
- Koppes, M., Hallet, B., Rignot, E., Mouginot, J., Wellner, J. S., & Boldt, K. (2015). Observed latitudinal variations in erosion as a function of glacier dynamics. *Nature*, 526(7571), 100–103. https://doi.org/10.1038/nature15385
- Koppes, M. N., & Montgomery, D. R. (2009). The relative efficacy of fluvial and glacial erosion over modern to orogenic timescales. *Nature Geoscience*, 2(9), 644–647. https://doi.org/10.1038/ngeo616
- Lane, S. N., Bakker, M., Gabbud, C., Micheletti, N., & Saugy, J.-N. (2017). Sediment export, transient landscape response and catchment-scale connectivity following rapid climate warming and Alpine glacier recession. *Geomorphology*, 277, 210–227. https://doi.org/10.1016/j. geomorph.2016.02.015
- Lenard, S. J. P., Lavé, J., France-Lanord, C., Aumaître, G., Bourlès, D. L., & Keddadouche, K. (2020). Steady erosion rates in the Himalayas through late Cenozoic climatic changes. *Nature Geoscience*, 13(6), 1–5. https://doi.org/10.1038/s41561-020-0585-2
- Leonard, E. M. (1997). The relationship between glacial activity and sediment production: Evidence from a 4450-year varve record of neoglacial sedimentation in Hector Lake, Alberta, Canada. *Journal of Paleolimnology*, 17, 319–330. https://doi.org/10.1023/A:1007948327654
- Livers, B., & Wohl, E. (2015). An evaluation of stream characteristics in glacial versus fluvial process domains in the Colorado Front Range. Geomorphology, 231, 72–82. https://doi.org/10.1016/j.geomorph.2014.12.003
- MacGregor, K. R., Anderson, R. S., Anderson, S. P., & Waddington, E. D. (2000). Numerical simulations of glacial-valley longitudinal profile evolution. Geology, 28(11), 1031–1034. https://doi.org/10.1130/0091-7613(2000)28<1031:NSOGLP>2.0.CO;2
- Malatesta, L. C., Avouac, J.-P., Brown, N. D., Breitenbach, S. F. M., Pan, J., Chevalier, M.-L., et al. (2018). Lag and mixing during sediment transfer across the Tian Shan piedmont caused by climate-driven aggradation–incision cycles. *Basin Research*, 30(4), 613–635. https://doi.org/10.1111/bre.12267
- Meyer-Peter, E., & Müller, R. (1948). Formulas for bed-load transport. IAHR.
- Mitchell, S. G., & Montgomery, D. R. (2006). Influence of a glacial buzzsaw on the height and morphology of the Cascade Range in central Washington State, USA. *Quaternary Research*, 65(1), 96–107. https://doi.org/10.1016/j.yqres.2005.08.018
- Molnar, P. (2004). Late cenozoic increase in accumulation rates of terrestrial sediment: How might climate change have affected erosion rates? Annual Review of Earth and Planetary Sciences, 32(1), 67–89. https://doi.org/10.1146/annurey.earth.32.091003.143456
- Montgomery, D. R., Balco, G., & Willett, S. D. (2001). Climate, tectonics, and the morphology of the Andes. *Geology*, 29(7), 579–582. https://doi.org/10.1130/0091-7613(2001)029<0579:CTATMO>2.0.CO;2
- Oerlemans, J. (1984). Numerical experiments on large-scale glacial erosion. Zeitschriftfür Gletscherkunde und Glazialgeologie, 20, 107–126. Pan, B., Burbank, D., Wang, Y., Wu, G., Li, J., & Guan, Q. (2003). A 900 k.y. record of strath terrace formation during glacial-interglacial transitions in northwest China. Geology, 31(11), 957–960. https://doi.org/10.1130/G19685.1
- Pazzaglia, F. J., & Brandon, M. T. (2001). A fluvial record of long-term steady-state uplift and erosion across the Cascadia Forearc High, Western Washington state. *American Journal of Science*, 301(4–5), 385–431. https://doi.org/10.2475/ajs.301.4-5.385
- Pedersen, V. K., & Egholm, D. L. (2013). Glaciations in response to climate variations preconditioned by evolving topography. *Nature*, 493(7431), 206–210. https://doi.org/10.1038/nature11786
- Pedersen, V. K., Egholm, D. L., & Nielsen, S. B. (2010). Alpine glacial topography and the rate of rock column uplift: A global perspective. Geomorphology, 122(1–2), 129–139. https://doi.org/10.1016/j.geomorph.2010.06.005

SCHANZ AND YANITES 15 of 16

- Peizhen, Z., Molnar, P., & Downs, W. R. (2001). Increased sedimentation rates and grain sizes 2–4 Myr ago due to the influence of climate change on erosion rates. *Nature*, 410(6831), 891–897. https://doi.org/10.1038/35073504
- Pollard, D., & DeConto, R. M. (2012). Description of a hybrid ice sheet-shelf model, and application to Antarctica. Geoscientific Model Development, 5, 1273–1295. https://doi.org/10.5194/gmd-5-1273-2012
- Rowley, D. B. (2002). Rate of plate creation and destruction: 180 Ma to present. GSA Bull, 114(8), 927–933. https://doi.org/10.1130/0016-7606 (2002)114<0927:ROPCAD>2.0.CO;2
- Sadler, P. M. (1981). Sediment accumulation rates and the completeness of stratigraphic sections. *The Journal of Geology*, 89(5), 569–584. https://doi.org/10.1086/628623
- Sadler, P. M., & Jerolmack, D. J. (2015). Scaling laws for aggradation, denudation and progradation rates: The case for time-scale invariance at sediment sources and sinks. Geological Society, London, Special Publications, 404(1), 69–88. https://doi.org/10.1144/SP404.7
- Schanz, S. (2024). schanzs/glacial-fluvial: RanGEs first release. [Software]. https://doi.org/10.5281/zenodo.10732828
- Schanz, S., & Yanites, B. (2024). Glacial fluvial simulation results for Schanz and Yanites. [Dataset]. https://doi.org/10.5281/zenodo.10719674
  Schanz, S. A., Montgomery, D. R., Collins, B. D., & Duvall, A. R. (2018). Multiple paths to straths: A review and reassessment of terrace genesis.

  Geomorphology, 312, 12–23. https://doi.org/10.1016/j.geomorph.2018.03.028
- Shobe, C. M., Tucker, G. E., & Barnhart, K. R. (2017). The SPACE 1.0 model: A Landlab component for 2-D calculation of sediment transport, bedrock erosion, and landscape evolution. *Geoscientific Model Development*, 10(12), 4577–4604. https://doi.org/10.5194/gmd-10-4577-2017
- Shuster, D. L., Ehlers, T. A., Rusmoren, M. E., & Farley, K. A. (2005). Rapid glacial erosion at 1.8 Ma revealed by 4He/3He thermochronometry. Science, 310(5754), 1668–1670. https://doi.org/10.1126/science.1118519
- Sklar, L. S., & Dietrich, W. E. (2001). Sediment and rock strength controls on river incision into bedrock. *Geology*, 29(12), 1087–1090. https://doi.org/10.1130/0091-7613(2001)029<1087:SARSCO>2.0.CO;2
- Sklar, L. S., & Dietrich, W. E. (2004). A mechanistic model for river incision into bedrock by saltating bed load. Water Resources Research, 40(6). https://doi.org/10.1029/2003WR002496
- Sternberg, H. (1875). Untersuchungen uber Langen-und Querprofil geschiebefuhrender Flusse. Zeitshrift Bauwes, 25, 483-506.
- Swift, D. A., Cook, S. J., Graham, D. J., Midgley, N. G., Fallick, A. E., Storrar, R., et al. (2018). Terminal zone glacial sediment transfer at a temperate overdeepened glacier system. *Quaternary Science Reviews*, 180, 111–131. https://doi.org/10.1016/j.quascirev.2017.11.027
- Van Der Meer, D. G., Zeebe, R. E., van Hinsbergen, D. J. J., Sluijs, A., Spakman, W., & Torsvik, T. H. (2014). Plate tectonic controls on atmospheric CO2 levels since the Triassic. Proceedings of the National Academy of Sciences of the United States of America, 111, 4380–4385. https://doi.org/10.1073/pnas.1315657111
- Whipple, K. X. (2009). The influence of climate on the tectonic evolution of mountain belts. *Nature Geoscience*, 2, 97–104. https://doi.org/10.1038/ngeo413
- Whipple, K. X., Hancock, G. S., & Anderson, R. S. (2000). River incision into bedrock: Mechanics and relative efficacy of plucking, abrasion, and cavitation. Geological Society of America Bulletin, 112(3), 490–503. https://doi.org/10.1130/0016-7606(2000)112<490:RIIBMA>2.0.CO;2
- Whipple, K. X., & Tucker, G. E. (1999). Dynamics of the stream-power river incision model: Implications for height limits of mountain ranges, landscape response timescales, and research needs. *Journal of Geophysical Research*, 104(B8), 17661–17674. https://doi.org/10.1029/100018000120
- Willenbring, J. K., & Jerolmack, D. J. (2016). The null hypothesis: Globally steady rates of erosion, weathering fluxes and shelf sediment accumulation during Late Cenozoic mountain uplift and glaciation. Terra Nova, 28(1), 11–18. https://doi.org/10.1111/ter.12185
- Willenbring, J. K., & von Blanckenburg, F. (2010). Long-term stability of global erosion rates and weathering during late-Cenozoic cooling. Nature, 465(7295), 211–214. https://doi.org/10.1038/nature09044
- Wong, M., & Parker, G. (2006). Reanalysis and correction of bed-load relation of Meyer-Peter and Müller using their own database. *Journal of Hydraulic Engineering*, 132(11), 1159–1168. https://doi.org/10.1061/(ASCE)0733-9429(2006)132:11(1159)
- Yanites, B. J. (2018). The dynamics of channel slope, width, and sediment in actively eroding bedrock river systems. J. Geophys. Res. Earth Surface, 123(7), 1504–1527. https://doi.org/10.1029/2017JF004405
- Zoet, L. K., & Iverson, N. R. (2020). A slip law for glaciers on deformable beds. Science, 368(6486), 76–78. https://doi.org/10.1126/science.

SCHANZ AND YANITES 16 of 16